Available online at www.sciencedirect.com
ScienceDirect
ELSEVIER
International Journal of Impact Engineering 34 (2007) 232–252
INTERNATIONAL JOURNAL OF IMPACT ENGINEERING
www.elsevier.com/locate/ijimpeng

Mechanism of buckling development in elastic bars subjected to axial impact

Anwen Wang*, Wenying Tian

Teaching and Research Section of Material Mechanics, PO. Box 0116, The Naval Academy of Engineering, Wuhan, 430033, People's Republic of China

Received 22 February 2005; received in revised form 4 July 2005; accepted 7 July 2005
Available online 12 September 2005

Abstract

By use of the finite difference method, the non-linear equations governing the elastic dynamic post-buckling deformations are solved for two types of impact buckling problems for straight bars. The initial dynamic buckling mode with a small amplitude parameter, given by the twin-characteristic-parameter solution, is used as the initial condition of the non-linear post-buckling solution. Particular attention is paid to the mechanism of growth and spread of buckling deformation in the bar and the interaction between the axial stress wave and the buckling deformation in the process of impact. It is found that the initial buckling deflection with one half-wave, occurring near the impacted end, spreads forward and develops into the higher mode as the axial stress wave propagates in the bar. The theoretical results are in good agreement with the experimental results reported in the literatures.

Keywords: Elastic bars; Axial impact; Growth and spread of buckling; Twin characteristic parameter solution; Stress wave

1. Introduction

The buckling problem of straight bars subjected to dynamically axial loading has been studied by many investigators [1–19]. Meier [2] showed that a column acted upon by a suddenly applied axial load could withstand compressive stress much in excess of the static critical stress [14]. Test

*Corresponding author.

0734-743X/$ - see front matter © 2005 Elsevier Ltd. All rights reserved.
doi:10.1016/j.ijimpeng.2005.07.005

results for the axial impact buckling of the slender bar [9] have shown that the local buckling with a higher mode occurs near the impacted end of the bar when the impact velocity is high. The phenomenon of the local buckling deformation and the occurrence of the higher buckling mode in the slender bar impacted axially are mainly due to the effects of stress wave and structural inertia. Recently, Karagiozova and Jones [17], and Lepik [19] investigated, respectively, the influence of stress wave propagation on the elastic–plastic dynamic buckling of the bar under axial impact.

In Ref. [20], the mechanism of the dynamic buckling initiation for the straight bar was investigated on the basis of transformation and conservation of energy in the transient process of buckling initiation, with the effects of stress wave and structural inertia taken into account. By derivation, it was found that, in the transient process of buckling initiation, amount of the released compressive-deformation energy is equal to the sum of the buckling-deformation energy and the buckling kinetic energy of the bar. The buckling kinetic energy is related to the transverse inertia effect of the bar at the initial stage of the buckling. In Ref. [20], the linear method of determining quantitatively the relation between the axial stress and the critical buckling time was presented for the geometrically perfect bar. In the analysis, the axial stress and the exponential parameter of inertia terms in the stability equations were treated as the two undetermined characteristic parameters. Therefore, the method is termed the twin-characteristic-parameter solution. The similar method was applied to the analyses of plastic dynamic buckling for straight bars [21] and thick cylindrical shells [22], and of elastic dynamic buckling for thin cylindrical shells [23], respectively.

The numerical results given by the two-characteristic-parameter solution [20] show that the transverse inertia effect has an important influence on the dynamic buckling of the straight bar, resulting in the buckling stress much higher than that of the static buckling. From the numerical results [20], it is found that under the same axial stress, the shortest critical buckling time is always related to the first buckling mode with one half-wave. Therefore, according to the theoretical prediction, the dynamic buckling of the straight bar is always initiated with the first buckling mode. From the high-speed photographs of the buckling deformation of a thin aluminum alloy strip under axial impact [13], it seems that the higher mode reported by the experimental investigation is the result of the development of the lower-mode buckling deformation.

By use of the linear method in Ref. [20], we obtain the pattern of the infinitesimal buckling deformation at the initial stage of dynamic buckling, but we cannot obtain any information on the mechanism of buckling deformation development and the pattern of the post-buckling deformation. Only by solving the non-linear equations governing the dynamic post-buckling deformation, we can obtain the pattern of the post-buckling deformation in the finite deformation state of the bar. In most literatures on the non-linear dynamic buckling response of the bar impacted axially, an initial geometrical imperfection in the shape of a half sine wave is taken as the initial condition of the non-linear solution. Obviously, it is not applicable to the bar without initial imperfection. Instead of it, in the present analysis, the initial buckling mode with a small amplitude parameter, given by the twin-characteristic-parameter solution, is adopted as the initial condition of the solution of the non-linear dynamic equations.

In this paper, the non-linear equations governing the elastic dynamic post-buckling deformations are solved for the two types of axial impact buckling problems of straight bars. Particular attention is paid to the mechanism of growth and spread of buckling deformation in the bar and the interaction between the axial stress wave and the buckling deformation in the process

of the impact. It is found that the initial buckling deflection with one half-wave, occurring near the impacted end, spreads forward and develops into the higher mode as the axial stress wave propagates. The obvious unloading of the axial stress wave appears in the region near the impacted end when the buckling deformation becomes large enough in this region. For the bar impacted axially by a striking mass, the buckling deformation decreases largely the loading duration and the values of the axial stress in the bar, in comparison with the case where there is no buckling deformation in the bar. The theoretical results are in good agreement with the experimental results reported in the literatures [9,13].

In the following, we first discuss the axial stress wave in the bar produced by axial impact, and then outline, in Section 2, the results given by the twin-characteristic-parameter solution for the critical state and the initial buckling mode. After that, in Section 4, we will carry out the finite difference solution of the nonlinear equations for the post-buckling deformation of the bar. Finally, the numerical results will be given in Section 5.

2. Stress wave in elastic bars produced by axial impact

In this section, we deal with the axial stress wave in the straight bar under the axial impacts of two types. The first type, as shown in Fig. 1(a), is that a straight bar traveling with the initial velocity v_0 is impacted against a rigid wall. The second is that an initially stationary bar is impacted by a mass M with the initial velocity v_0, as shown in Fig. 1(b).

2.1. The axial stress wave in the bar impacted against a rigid wall

As shown in Fig. 1(a), the straight bar is originally stress-free and moving toward a rigid wall, with velocity v_0. On impact the left end of the bar immediately come to rest. Adjacent particles to the right come to rest later as the stress wave of magnitude σ propagates to the right at the sound velocity c of the bar material. After the time interval t, the stress wave has passed a distance $x_\sigma = ct$ into the bar, and the impulse applied by the end load at the rigid wall must be equal to the

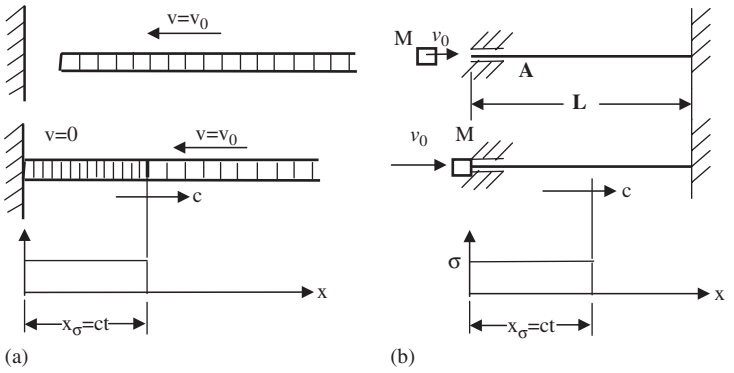

Fig. 1. (a) Axial stress wave in a bar impacting against a rigid wall. (b) Axial stress wave in a bar impacted by a traveling mass.

initial momentum of the length x_σ brought to rest by the stress wave. From this condition, we obtain the axial compressive stress in the bar:

$$\sigma = \rho c v_0 \quad (0 \leqslant x < x_\sigma), \tag{2.1a}$$

$$\sigma = 0 \quad (x_\sigma < x \leqslant L), \tag{2.1b}$$

where ρ is the density of the bar material.

For the bar impacted against a rigid wall as shown in Fig. 1(a), our discussion is limited to the case where the axial stress wave has not arrived at the free end. In Fig. 1(a), the axial displacement of the bar is taken positive towards the right, and expressed as

$$u_0 = -\frac{x}{c} v_0 \quad (0 \leqslant x \leqslant x_\sigma), \tag{2.2a}$$

$$u_0 = -v_0 t \quad (x_\sigma \leqslant x \leqslant L). \tag{2.2b}$$

2.2. The axial stress wave in the bar impacted by a striking mass

As shown in Fig. 1(b), the stationary bar is fixed at the right end, and is impacted axially at the left end by a mass M traveling with an initial velocity v_0. Assuming that the impact begins at the instant $t = 0$, at instant $t > 0$ the axial motion equation of the straight bar without buckling deformation, is written as

$$E u_{0,xx} = \rho u_{0,tt}, \tag{2.3}$$

where u_0 denotes the axial displacement of the bar, and E is Young's modulus of the bar material. Before the axial stress wave arrives at the fixed end, Eq. (2.3) is valid for the region $0 \leqslant x \leqslant ct$. The boundary condition at the front of the axial stress wave is written as

$$u_0(x, t)|_{x=ct} = 0. \tag{2.4a}$$

After the axial stress wave arrives at the fixed end, Eq. (2.3) is valid for the region $0 \leqslant x \leqslant L$. Then, the boundary condition (2.4a) is replaced by

$$u_0(x, t)|_{x=L} = 0. \tag{2.4b}$$

Before the striking mass M separates from the bar, the boundary condition at the impacted end is expressed by

$$\{AE u_{0,x} - M u_{0,tt}\}_{x=0} = 0, \tag{2.5}$$

where A is the area of the cross section of the bar. Assuming that M is a rigid striking mass, the initial conditions are written as

$$u_0(x, 0) = 0, \tag{2.6}$$

$$u_{0,t}|_{x=0,t=0} = v_0, \tag{2.7a}$$

$$u_{0,t}|_{x>0,t=0} = 0. \tag{2.7b}$$

The differential Eq. (2.3) is solved by use of the finite central difference method, and the difference equation corresponding to the reference point (x, t) is written as

$$u_0(x, t+\Delta t) = \left(\frac{c\,\Delta t}{\Delta x}\right)^2 (u_0(x+\Delta x, t) - 2u_0(x, t) + u_0(x-\Delta x, t)) + 2u_0(x, t) - u_0(x, t-\Delta t). \tag{2.8}$$

The difference equation for the boundary condition (2.5) and the initial condition (2.7) are, respectively,

$$u_0(0, t+\Delta t) = \frac{AE}{M}\frac{(\Delta t)^2}{\Delta x}[u_0(\Delta x, t) - u_0(0, t)] + 2u_0(0, t) - u_0(0, t-\Delta t)(t \geqslant \Delta t), \tag{2.9}$$

$$u_0(0, \Delta t) = v_0 \Delta t, \tag{2.10a}$$

$$u_0(x, \Delta t)|_{x>0} = 0. \tag{2.10b}$$

Considering that the axial stress wave propagates forward at the rate c, let $\Delta x = c\,\Delta t$ in the calculation and the convergent numerical results are obtained. At the initial stage of the impact, the load-time history at the impacted end may be treated approximately as the step loading with an invariable magnitude, as shown in Fig. 1(b).

3. Critical buckling time and initial buckling mode

If the slenderness ratio of the impacted bar is large enough and the impact velocity v_0 is high, at the early stage of impact loading, the buckling deformation will occur in the portion of the bar covered by the axial stress wave. At this stage, the axial stress wave produced at the impacted end has not arrived at the other end of the bar.

Assuming that the bar begins to be impacted at the instant $t = 0$, the instant when an infinitesimal buckling deflection occurs in the bar is defined as the critical buckling time t_{cr}. At this instant, the length of the portion covered by the axial stress wave is equal to $L_{cr} = ct_{cr}$, which is defined as the critical buckling length. The deformation pattern corresponding to the infinitesimal buckling deflection, with an undetermined amplitude parameter, is given by the twin-characteristic-parameter solution of Ref. [20], which is called the dynamic buckling mode. The numerical results of Ref. [20] show that, owing to the effect of the transverse inertia, the dynamic buckling mode is different from the static buckling mode of the bar with same cross-section and the length $L_s = L_{cr}$. The relations between the axial compressive stress σ_{cr} and the critical buckling time t_{cr}, corresponding to the different dynamic buckling modes, are given by the twin-characteristic-parameter solution of Ref. [20]. Under the same axial stress, the shortest critical buckling time is corresponding to the first dynamic buckling mode. From the Eq. (6.3) in Ref. [20], the relation between σ_{cr} and t_{cr} for the first dynamic buckling mode is expressed by

$$\sigma_{cr} = \frac{N_{cr}^{(1)}}{A} = \frac{\Lambda_1^{(1)} EI}{Ac^2 t_{cr}^2}, \tag{3.1}$$

where $N_{cr}^{(1)}$ is the critical compressive force in the bar related to the first buckling mode, $\Lambda_1^{(1)}$ is the critical stress parameter defined in Ref. [20], in which the superscript (1) denotes that it corresponds to the first dynamic buckling mode, and I is the inertial moment of the cross-section of the bar. Eq. (3.1) is re-written as

$$L_{cr} = \sqrt{\frac{\Lambda_1^{(1)} E}{\sigma_{cr}}} r, \tag{3.2a}$$

$$t_{cr} = \frac{L_{cr}}{c}, \tag{3.2b}$$

where r is the gyration radius of the cross-section. For a slender bar impacted at high velocity, the critical buckling length L_{cr} is much shorter than the total length L of the bar. For the case where at the impacted end, the deflection and rotation of the bar is restrained completely but the axial displacement is allowed, which are call the loose clamp conditions, the value of the parameter $\Lambda_1^{(1)}$ given by Ref. [20] is

$$\Lambda_1^{(1)} = 10\pi^2. \tag{3.3a}$$

For the case where the bar is simply supported at the impacted end,

$$\Lambda_1^{(1)} = 5\pi^2. \tag{3.3b}$$

Let w_0 denote the initial buckling deflection. From the twin-characteristic-parameter solution of Ref. [20], the expression of the dimensionless deflection $\bar{w}_0$ corresponding to the first dynamic buckling mode is written as

$$\bar{w}_0 = \frac{w_0}{r} = \mu e^{\omega(\tau-1)} Y(\xi). \tag{3.4}$$

For the loose clamp condition at the impacted end,

$$Y(\xi) = 3\sin(\pi\xi) - \sin(3\pi\xi). \tag{3.5a}$$

For the simple support condition at the impacted end,

$$Y(\xi) = 2\sin(\pi\xi) + \sin(2\pi\xi). \tag{3.5b}$$

In Eq. (3.4), μ is an undetermined small magnitude parameter, and the other dimensionless parameters are defined by the following equations:

$$\omega = \frac{r\Lambda_2^{(1)}}{L_{cr}}, \tag{3.6a}$$

$$\tau = \frac{t}{t_{cr}}, \tag{3.6b}$$

$$\xi = \frac{x}{L_{cr}}. \tag{3.6c}$$

In Eq. (3.6a), $\Lambda_2^{(1)}$ is the inertial exponential parameter corresponding to the first dynamic buckling mode, which was termed the dimensionless dynamic characteristic parameter in Ref. [20]). According to the solution of Ref. [20], $\Lambda_2^{(1)} = 3\pi^2$ for the loose clamp boundary

condition at the impacted end, and $\Lambda_2^{(1)} = 2\pi^2$ for the simple support boundary condition at the impacted end. The dynamic buckling mode (3.4) satisfies the following restraint conditions at the front of the axial stress wave:

$$\bar{w}_0(\xi,\tau)|_{\xi=1,\tau=1} = 0, \tag{3.7a}$$

$$\bar{w}_{0,\xi}|_{\xi=1,\tau=1} = 0, \tag{3.7b}$$

$$\bar{w}_{0,\xi\xi}|_{\xi=1,\tau=1} = 0, \tag{3.7c}$$

where Eq. (3.7c) is the supplementary restraint condition, at the front of the axial stress wave and at the critical buckling instant $\tau = 1$ ($t = t_{cr}$), obtained by use of the criterion of transformation and conservation of energy in the transient process of buckling initiation.

4. Dynamic post-buckling equations and their difference solution

4.1. The equations of post-buckling motion for the axially impacted bar

If the dynamic buckling occurs at the early stage of the impact loading, the buckling deformation will develop rapidly with the propagation of axial stress wave in the process of impact loading. For the elastic dynamic buckling of a slender bar, the effects of shear deformation and rotary inertia are negligible, and the non-linear motion equations of the bar after buckling are written as

$$N_{x,x} - \rho A u_{,tt} = 0, \tag{4.1}$$

$$M_{x,xx} - (N_x w_{,x})_{,x} + \rho A w_{,tt} = 0, \tag{4.2}$$

where N_x is the axial force, M_x is the bending moment, u denotes the total axial-displacement after the buckling occurs, and w is the lateral displacement corresponding to the buckling deformation. For the elastic bar, N_x and M_x are related to the centroidal-surface strain ε_x and the curvature κ by the following expressions, respectively:

$$N_x = AE\varepsilon_x, \tag{4.3a}$$

$$M_x = EI\kappa. \tag{4.3b}$$

The deformation–displacement relations are expressed by

$$\varepsilon_x = u_{,x} + \tfrac{1}{2} w_{,x}^2, \tag{4.4a}$$

$$\kappa = \frac{w_{,xx}}{(1 + w_{,x}^2)^{3/2}}. \tag{4.4b}$$

For the convenience of analysis, we write the displacement components u and w into the dimensionless forms:

$$\bar{u} = \frac{L_{cr}}{r}\frac{u}{r}, \tag{4.5a}$$

$$\bar{w} = \frac{w}{r}. \tag{4.5b}$$

With Eqs. (4.3)–(4.5) introduced, the Eqs. (4.1) and (4.2) are transformed into

$$\bar{u}_{,\xi\xi} + \bar{w}_{,\xi}\bar{w}_{,\xi\xi} = \bar{u}_{,\tau\tau}, \tag{4.6}$$

$$\bar{w}_{,\xi\xi\xi\xi}\left(1 - \frac{3}{2}\bar{r}^2\bar{w}_{,\xi}^2\right) - 3\bar{r}^2\bar{w}_{,\xi\xi}^3 - 9\bar{r}^2\bar{w}_{,\xi}\bar{w}_{,\xi\xi}\bar{w}_{,\xi\xi\xi} - \bar{u}_{,\xi\xi}\bar{w}_{,\xi} - \bar{u}_{,\xi}\bar{w}_{,\xi\xi} - \frac{3}{2}\bar{w}_{,\xi}^2\bar{w}_{,\xi\xi} + \frac{1}{\bar{r}^2}\bar{w}_{,\tau\tau} = 0, \tag{4.7}$$

where $\bar{r} = r/L_{cr}$. According to Eq. (3.2a), the value of the parameter $\bar{r}$ is far smaller than the unit 1 for the elastic buckling of a slender bar. In the derivation of Eq. (4.7), we have omitted the terms containing the power $\bar{r}^n$ for which $n \geqslant 3$.

4.2. The initial conditions for the solution of post-buckling motion equations

As mentioned in Section 3, the instant when the infinitesimal buckling deformation occurs is defined as the critical buckling time $t = t_{cr}$, at which $\tau = t/t_{cr} = 1$. Therefore, the axial displacement u_0 at the instant $t = t_{cr}$, given by the solution in Section 2, and the initial buckling deflection w_0 expressed by Eq. (3.4) are taken as the initial values of the post-buckling displacements u and w, respectively. The initial conditions for the displacement w in the dimensionless forms are expressed by

$$\bar{w}|_{\tau=1} = \bar{w}_0, \tag{4.8a}$$

$$\bar{w}_{,\tau}\big|_{\tau=1} = \bar{w}_{0,\tau} \quad (0 \leqslant \xi \leqslant 1), \tag{4.8b}$$

$$\bar{w}|_{\tau=1} = 0, \tag{4.9a}$$

$$\bar{w}_{,\tau}\big|_{\tau=1} = 0 \quad (1 \leqslant \xi \leqslant L/L_{cr}), \tag{4.9b}$$

where the expression of $\bar{w}_0$ is given by Eq. (3.4).

In the case where the bar is impacted against a rigid wall, as shown in Fig. 1(a), the value of axial displacement u at the instant $t = t_{cr}$ is obtained from Eqs. (2.2a,b). The initial value at the instant $t = t_{cr}$ for the axial post-buckling displacement u are written as

$$u(x,t)|_{t=t_{cr}} = -\frac{x}{c}v_0 \quad (0 \leqslant x \leqslant L_{cr}), \tag{4.10a}$$

$$u(x,t)|_{t=t_{cr}} = -v_0 t_{cr} \quad (L_{cr} \leqslant x \leqslant L), \tag{4.10b}$$

$$u_{,t}|_{t=t_{cr}} = 0, \quad 0 \leqslant x < L_{cr}, \tag{4.10c}$$

$$u_{,t}|_{t=t_{cr}} = -v_0 \quad (L_{cr} < x \leqslant L). \tag{4.10d}$$

By use of Eqs. (2.1a), (3.1), (3.6b,c) and (4.5a), the initial conditions (4.10a–d) are re-written into the following dimensionless forms

$$\bar{u}(\xi,\tau)|_{\tau=1} = -\Lambda_1^{(1)}\xi \quad (0 \leqslant \xi \leqslant 1), \tag{4.11a}$$

$$\bar{u}(\xi,\tau)|_{\tau=1} = -\Lambda_1^{(1)} \quad (1 \leqslant \xi \leqslant L/L_{cr}), \tag{4.11b}$$

$$\bar{u}_{,\tau}|_{\tau=1} = 0 \quad (0 \leqslant \xi < 1), \tag{4.11c}$$

$$\bar{u}_{,\tau}|_{\tau=1} = -\frac{L_{cr} t_{cr}}{r^2} v_0 \quad (1 < \xi \leqslant L/L_{cr}). \tag{4.11d}$$

For the case where the stationary bar is impacted at the left end by a striking mass M, as shown in Fig. 1(b), the values of the dimensionless displacement $\bar{u}$ and its derivative $\bar{u}_{,\tau}$ at the initial instant $\tau = 1 (t = t_{cr})$ are obtained by use of the solution of the difference Eq. (2.8) in Section 2.2 and the expression (4.5a).

4.3. Boundary conditions for the solution of post-buckling motion equations

4.3.1. Boundary conditions at the impacted end

For the bar impacted against a rigid wall as shown in Fig. 1(a), in order to compare the present theoretical results with the experimental results of Ref. [13] where the specimen was clamped at the impacted end by the lower jaw of the tensile testing machine, the boundary conditions at the impacted end are written as

$$\bar{u}(0, \tau) = 0, \tag{4.12a}$$

$$\bar{w}(0, \tau) = 0, \tag{4.12b}$$

$$\bar{w}_{,\xi}|_{\xi=0} = 0. \tag{4.12c}$$

For the initially stationary bar impacted by a traveling mass, the axial boundary condition at the impacted end, before the separation of the striking mass from the impacted end, is obtained by use of the motion equation of the striking mass M. After derivation, it is written as

$$\bar{u}_{,\tau\tau}|_{\xi=0} = \frac{AEt_{cr}^2}{ML_{cr}} \left(\bar{u}_{,\xi} + \frac{1}{2} \bar{w}_{,\xi}^2 \right)_{\xi=0}. \tag{4.13}$$

For the case where the transverse displacement and rotation of the impacted end of the bar are restrained completely in the process of impact, the boundary conditions at the impacted end for the displacement $\bar{w}$ are the same as Eqs. (4.12b,c). If the bar is simply supported at the impacted end, the boundary conditions for the displacement $\bar{w}$ will be

$$\bar{w}(0, \tau) = 0, \tag{4.14a}$$

$$\bar{w}_{,\xi\xi}|_{\xi=0} = 0. \tag{4.14b}$$

4.3.2. Boundary conditions at the front of compressive wave or at the fixed end

For the slender bar impacted against a rigid wall, as shown in Fig. 1(a), the present analysis is limited to the buckling deformation stage at which the axial stress wave has not arrive at the free end. The front of the axial stress wave is one of the two boundaries of the buckling deformation region. The boundary conditions at the stress wave front ($x = ct$ or $\xi = \tau$) are written as

$$\bar{u}(\xi, \tau)|_{\xi=\tau} = -\left(\frac{L_{cr}}{r} \right)^2 \frac{v_0 \tau}{c_0}, \tag{4.15a}$$

$$\bar{w}(\xi,\tau)|_{\xi=\tau}=0, \tag{4.15b}$$

$$\bar{w}_{,\xi}|_{\xi=\tau}=0. \tag{4.15c}$$

For the initially stationary bar impacted by a striking mass, as shown in Fig. 1(b), the boundary conditions at the front of the stress wave is the same as Eqs. (4.15a–c) before the axial stress wave arrives at the fixed end. After the axial stress wave arrives at the fixed end, instead of the axial stress wave front, the fixed end becomes one of the two boundaries of the buckling deformation region. Assuming that the bar is clamped at the fixed end, the boundary conditions at the fixed end are written as

$$\bar{u}(\xi,\tau)|_{\xi=L/L_{cr}}=0, \tag{4.16a}$$

$$\bar{w}(\xi,\tau)|_{\xi=L/L_{cr}}=0, \tag{4.16b}$$

$$\bar{w}_{,\xi}|_{\xi=L/L_{cr}}=0. \tag{4.16c}$$

4.4. The finite difference solution of Eqs. (4.6) and (4.7)

The non-linear differential Eqs. (4.6) and (4.7) are solved by use of the finite central difference method. The central difference formulas corresponding to the reference point (ξ,τ) are expressed as

$$\frac{\partial\bar{u}(\xi,\tau)}{\partial\xi}=\frac{1}{2\Delta\xi}[\bar{u}(\xi+\Delta\xi,\tau)-\bar{u}(\xi-\Delta\xi,\tau)], \tag{4.17a}$$

$$\frac{\partial^2\bar{u}(\xi,\tau)}{\partial\xi^2}=\frac{1}{(\Delta\xi)^2}[\bar{u}(\xi+\Delta\xi,\tau)-2\bar{u}(\xi,\tau)+\bar{u}(\xi-\Delta\xi,\tau)], \tag{4.17b}$$

$$\frac{\partial\bar{w}(\xi,\tau)}{\partial\xi}=\frac{1}{2\Delta\xi}[\bar{w}(\xi+\Delta\xi,\tau)-\bar{w}(\xi-\Delta\xi,\tau)], \tag{4.17c}$$

$$\frac{\partial^2\bar{w}(\xi,\tau)}{\partial\xi^2}=\frac{1}{(\Delta\xi)^2}[\bar{w}(\xi+\Delta\xi,\tau)-2\bar{w}(\xi,\tau)+\bar{w}(\xi-\Delta\xi,\tau)], \tag{4.17d}$$

$$\frac{\partial^3\bar{w}(\xi,\tau)}{\partial\xi^3}=\frac{1}{(\Delta\xi)^3}\left[\frac{1}{2}\bar{w}(\xi+2\Delta\xi,\tau)-\bar{w}(\xi+\Delta\xi,\tau)+\bar{w}(\xi-\Delta\xi,\tau)-\frac{1}{2}\bar{w}(\xi-2\Delta\xi,\tau)\right], \tag{4.17e}$$

$$\frac{\partial^4\bar{w}(\xi,\tau)}{\partial\xi^4}=\frac{1}{(\Delta\xi)^4}[\bar{w}(\xi+2\Delta\xi,\tau)-4\bar{w}(\xi+\Delta\xi,\tau)+6\bar{w}(\xi,\tau)-4\bar{w}(\xi-\Delta\xi,\tau)+\bar{w}(\xi-2\Delta\xi,\tau)], \tag{4.17f}$$

$$\frac{\partial^2\bar{u}(\xi,\tau)}{\partial\tau^2}=\frac{1}{(\Delta\tau)^2}[\bar{u}(\xi,\tau+\Delta\tau)-2\bar{u}(\xi,\tau)+\bar{u}(\xi,\tau-\Delta\tau)], \tag{4.17g}$$

$$\frac{\partial^2 \bar{w}(\xi,\tau)}{\partial \tau^2} = \frac{1}{(\Delta\tau)^2}\left[\bar{w}(\xi,\tau+\Delta\tau) - 2\bar{w}(\xi,\tau) + \bar{w}(\xi,\tau-\Delta\tau)\right]. \tag{4.17h}$$

Introducing Eqs. (4.17a–h) into Eqs. (4.6) and (4.7), we obtain the central difference equations related to Eqs. (4.6) and (4.7). The differentiations with respect to the variable ξ or τ in the above-mentioned boundary conditions and initial conditions are also transformed into the corresponding difference formulas. Considering that the axial stress wave propagates at the rate c in the bar, in calculation we take $\Delta\xi = \Delta\tau$, that is $\Delta x = c\,\Delta t$, and obtain the convergent numerical results.

5. Numerical results

By use of the solution developed in the Sections 2–4, the elastic dynamic buckling and post-buckling are investigated for two types of the axial impacts of the straight bars, as shown in Fig. 1(a, b). Particular attention is paid to the mechanism of growth and spread of the dynamic buckling deformation in the bar and the interaction between axial stress wave and buckling deformation in the process of the impact. The numerical results are compared with the experimental results reported in Refs. [9,13].

5.1. The example of bar impacted against a rigid wall

In Refs. [8,13], the dynamic buckling experiment for a long bar to be impacted against a rigid wall, as shown in Fig. 1(a), was produced by using a tensile testing machine. The specimen, a strip made of aluminum alloy 6061-T6 with a 12.7 by 0.32 mm cross-section and a length of 726 mm, is clamped at both ends by the two jaws of the tensile testing machine. Before the tension is applied, a notch is filed in the trip near the upper jaw with its depth adjusted so that fracture occurs at the notch when the value of the stress σ in the remainder of the trip is approximately 276 MPa, which is below the yield stress $\sigma_s = 310$ MPa [13]. After fracture, a relief wave travels down the trip at velocity c, leaving the trip stress-free behind the wave and traveling at velocity $v_0 = \sigma/\rho c$. When the wave arrives at the lower jar it reflects again as a compressive wave. The stress caused by the compressive wave will be equal to the initial tensile stress $\sigma = 276$ MPa if the lower jar acts as a rigid wall.

The buckling deformations of the aluminum strip at different stages were photographed by use of an ultrahigh-speed framing camera, which were shown in Fig. 2.15 of Ref. [13]. The photographs show that the large deflection at the post-buckling stage is limited to a short portion of the trip close to the lower jaw. The length of the first buckling half-wave near the lower jaw, measured experimentally, is about 11.9 mm [13].

By use of the formulas developed in the Sections 2–4, we investigate numerically the dynamic buckling deformation of the aluminum alloy strip. The initial buckling mode calculated by use of Eqs. (3.4) and (3.5a), with the amplitude parameter $\mu = 0.005$, is shown in Fig. 2. In the calculation, the elastic modulus of the material is taken as $E = 68.5$ Gpa. For $\sigma_{cr} = 276$ MPa, the critical buckling length given by Eq. (3.2a) is $L_{cr} = 14.46$ mm, and the critical buckling time given by Eq. (3.2b) is about $t_{cr} = 2.89\,\mu s$. The distributions of the dimensionless post-buckling deflection $\bar{w}$ along the bar at the different instants from $\tau = 1.5$ to 16, given by the solution of

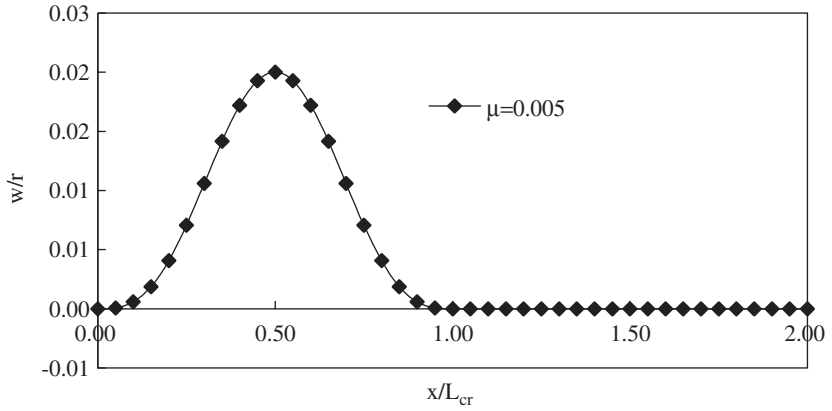

Fig. 2. Initial buckling mode of aluminum strip, $t_{cr} = 2.89\,\mu s$, $L_{cr} = 14.46\,mm$.

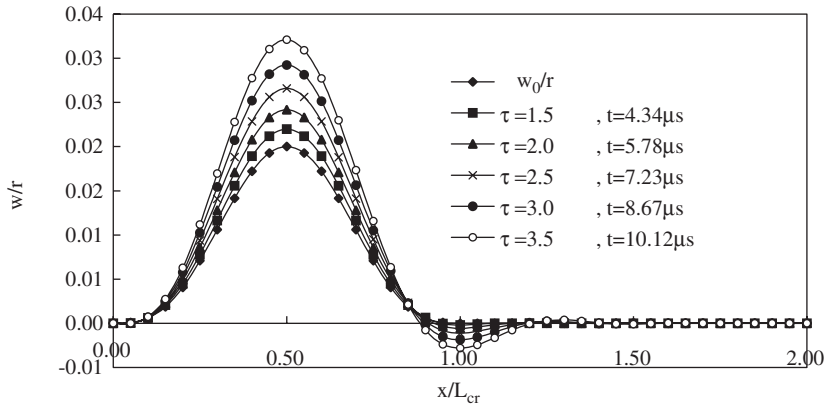

Fig. 3. Growth and spread of buckling deformation in aluminum strip, $\mu = 0.005$.

Section 4, are shown in Figs. 3–5, where $\mu = 0.005$. From Figs. 2–5, it can be seen that the initial buckling deformation, with one half-wave, near the impacted end spreads forward and develops into a series of higher post-buckling modes corresponding to the different stage, as the axial stress wave propagates towards the free end in the process of impact. At the post-buckling stage, the position $\xi = 1$, corresponding to front of the half-wave of the initial buckling mode, transformed into the wave-valley of the next half-wave of the post-buckling deflection mode, and then the half-wave of the post-buckling mode remains fixed in position and merely grows in amplitude. At the post-buckling stage, the length of the first half-wave close to the impacted end, of the buckling deflection profile, is approximately $0.783L_{cr} = 11.3\,mm$, which is shorter than the length $L_{cr} = 14.46\,mm$of the initial buckling mode. The value 11.3 mm is very close to the experimental value of 11.9 mm given by Ref. [13].

Form Figs. 3–5, it can be seen that the large buckling deformation are limited to a shorter region near the impact end, in comparison with the length of the portion covered by the axial

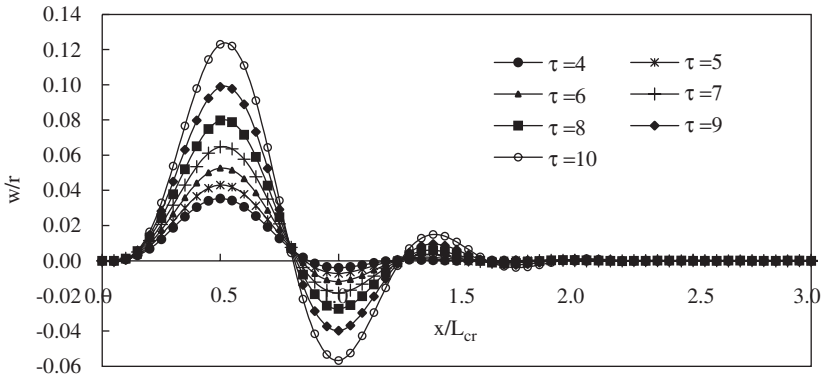

Fig. 4. Growth and spread of buckling deformation in aluminum strip, $\mu = 0.005$.

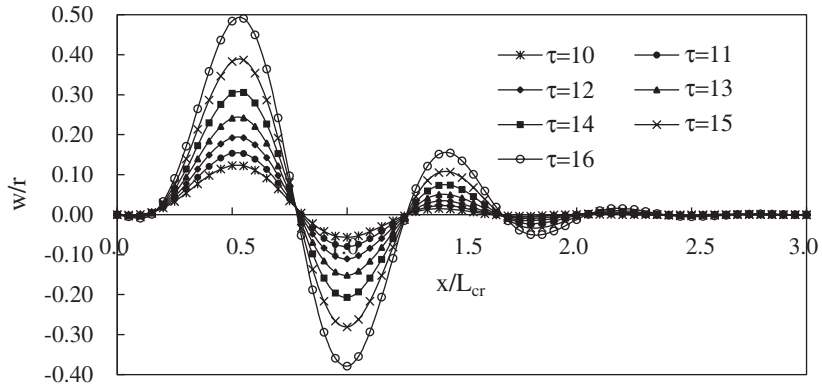

Fig. 5. Growth and spread of buckling deformation in aluminum strip, $\mu = 0.005$.

stress wave. For example, at the instant $\tau = t/t_{cr} = 16$, the length covered by the axial stress wave is equal to $L = 16L_{cr}$ (about 231 mm), whereas the length of the portion with visible buckling deformations in Fig. 5 is only about $2.5L_{cr}$ (about 36 mm), which is much shorter than the former. At the instants $\tau = 12$ and 16, the axial compressive stress and bending stress in the aluminum strip, given by the present calculation, are shown in the Figs. 6 and 7, respectively. It can be seen from Fig. 7 that, at the cross-section where the maximum bending moment appears, the sum of the axial stress and the maximum bending stress exceeds the value of the yield stress σ_s and the little part of material on the concave side of the aluminum strip undergoes plastic deformation. In this case, the actual buckling deflection in a region near the cross-section will be a little larger than the computed value.

The numerical results show that the value of the parameter μ in the expression (3.4) of the initial buckling mode has a considerable influence on the amplitude of post-buckling deflections at the given instant, but has little influence on the shape of the post-buckling deflection profile. For examples, as shown in Fig. 8, the post-buckling deflection profile for = 0.003 at the instant $\tau = 18$ almost coincides with that for $\mu = 0.005$ at $\tau = 16$.

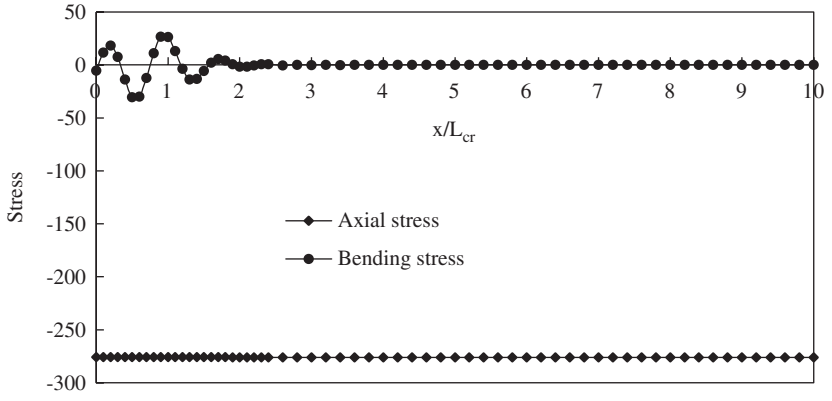

Fig. 6. Axial stress and bending stress in aluminum strip, $\mu = 0.005$, $\tau = 12$.

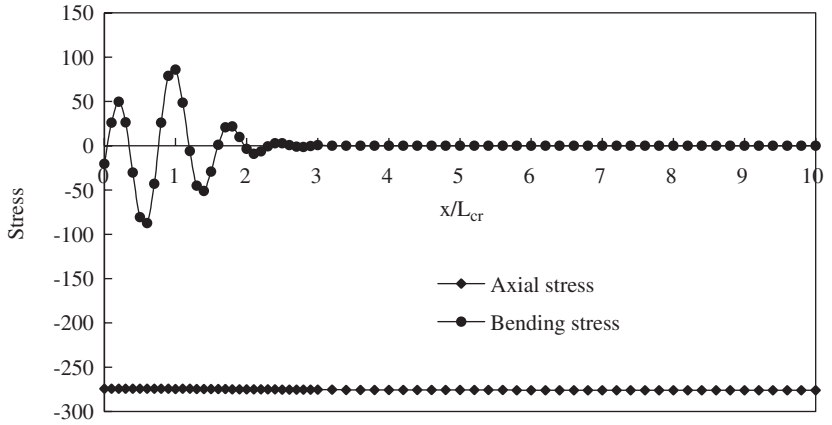

Fig. 7. Axial stress and bending stress in aluminum strip, $\mu = 0.005$, $\tau = 16$.

5.2. *The example of stationary bar impacted by a traveling mass*

A dynamic buckling experiment for the bar to be impacted axially by a mass traveling at a high velocity was reported by Ref. [9]. The specimens were made of Ni–Cr steel with Young's modulus $E = 210$ GPa, density $\rho = 7800\ \mathrm{kg/m^3}$, and yield stress $\sigma_s = 1500$ MPa. The specimens have length $l = 193$ mm and the rectangular cross-section of thickness $h = 0.63$ mm and width $b = 8.7$ mm. The weight of the striking mass is $M = 0.369$ kg. For the specimen No. 2, the initial velocity of the striking mass is $v_0 = 6.3$ m/s.

For comparison, the dynamic buckling of the above-mentioned specimen is investigated numerically by use of the solution in the Sections 2–4. In the present analysis, the bar is assumed to be geometrically perfect, which is different from Ref. [9] where the specimen was initially bent in the shape of a half sine wave. In the calculation, the bar is assumed to be simply supported at the impacted end, which is consistent with the experimental conditions of Ref. [9]. For the convenience of calculation, it is assumed the bar is clamped at the fixed end.

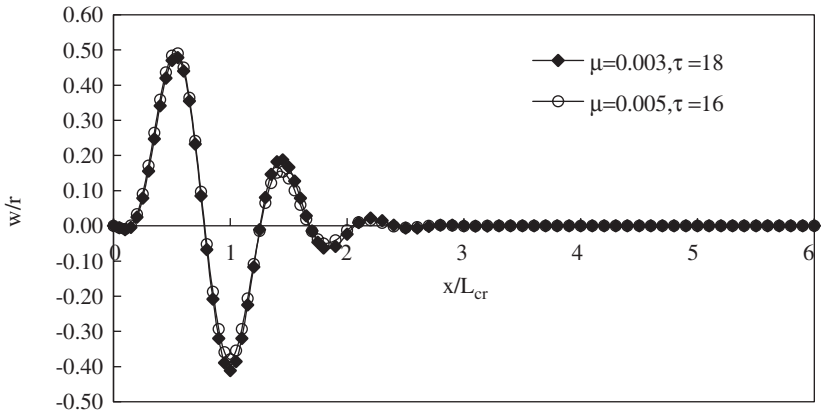

Fig. 8. Influence of the parameter μ on the buckling deflection of aluminum strip.

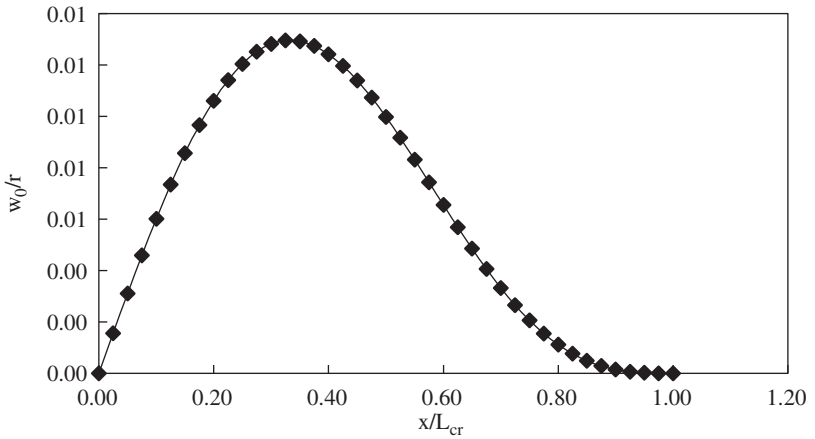

Fig. 9. Intial buckling mode of Ni–Cr steel bar, $v_0 = 6.3\,\mathrm{m/s}$, $\mu = 0.005$.

In the case where the bar is simply supported at the impacted end, we have the critical stress parameter $\Lambda_1^{(1)} = 5\pi^2$ from Eq. (3.3b). By use of Eq. (3.2), we obtain the critical buckling length $L_{cr} = 36.66$ mm and the critical buckling time $t_{cr} = 7.065\,\mu s$. The initial buckling mode calculated by use of Eqs. (3.4) and (3.5b), with the amplitude parameter $\mu = 0.005$, is shown in Fig. 9. The growth of the deflection $\bar{w}$ with the time t, given by the present calculation, are shown in Figs. 10–12, where $\mu = 0.005$. In a similar way to the buckling deformations of the aluminum strip mentioned above, the initial buckling deflection of the Ni–Cr steel bar with one half-wave, spreads towards the fixed end and develops into a series of higher modes, corresponding to the different stage, due to the propagation of the axial stress wave in the bar. The comparison between the post-buckling deflections for the different parameter μ, at the different times, is shown in Fig. 13. From Fig. 13, it can be seen that the amplitude parameter μ of the initial buckling deflection has little influence on the shape of the post-buckling mode, but it needs a longer time t for the initial

buckling mode with a smaller parameter μ to develop into the post-buckling mode with the same amplitude.

At several different instants $\tau = 3.5$, 23.5 and 26, the axial compression stresses and bending stresses in the specimen, obtained from the present calculation, are shown in Figs. 14–16, respectively. In the calculation, it is found that the maximum bending moment appears at the same position $\xi = x/L_{cr} = 0.275$ for the parameter $\mu = 0.001$, 0.002, 0.003, and 0.005, which is corresponding to the ratio $x/L = 0.05238$. The experimental result of Ref. [9] gives that the maximum bending stress appears at the position $x/L = 0.05$. Therefore, the present numerical result is in reasonable agreement with the experimental result of Ref. [9].

From Figs. 15 and 16, it can be seen that there is the unloading of the axial stress wave in the case where the post-buckling deformation develops large enough. The histories of axial stress σ vs. time t at the impacted end of the bar are shown in Fig. 17 for the different values of the parameter μ. Assuming that the buckling does not occur in the process of impact and the yield stress of the

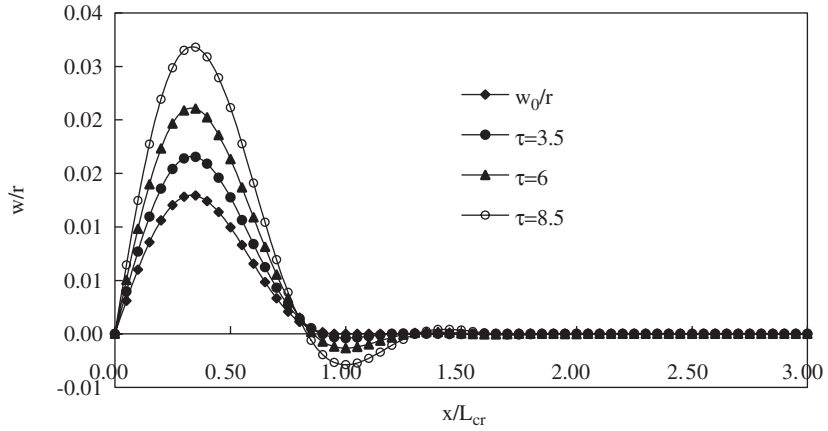

Fig. 10. Growth and spread of buckling deformation in Ni–Cr steel bar, $v_0 = 6.3\,\mathrm{m/s}$, $\mu = 0.005$.

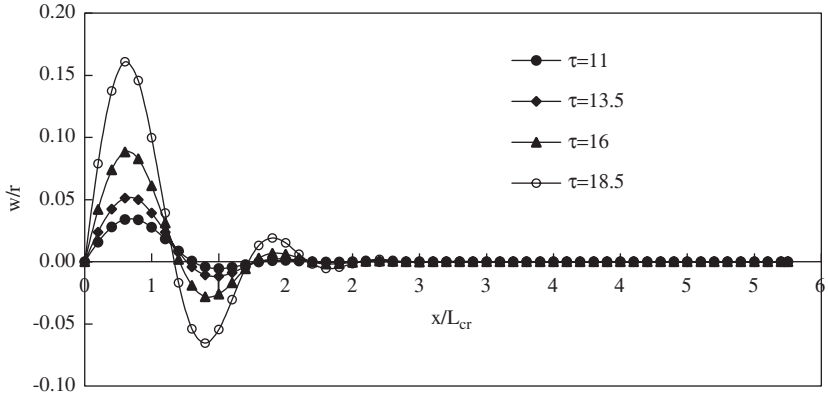

Fig. 11. Growth and spread of buckling deformation in Ni–Cr steel bar, $v_0 = 6.3\,\mathrm{m/s}$, $\mu = 0.005$.

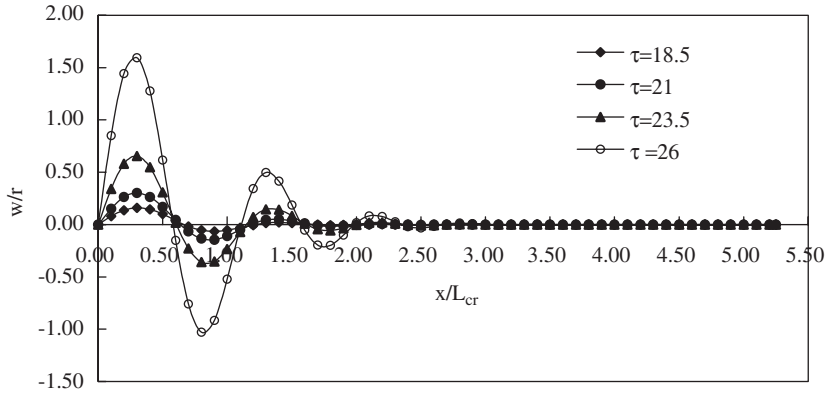

Fig. 12. Growth and spread of buckling deflection in Ni–Cr steel bar, $v_0 = 6.3\,\mathrm{m/s}$, $\mu = 0.005$.

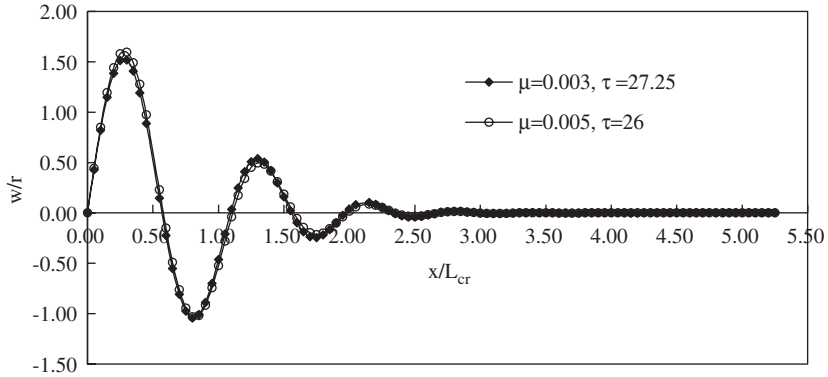

Fig. 13. Influence of the parameter μ on buckling deflection of Ni–Cr steel bar, $v_0 = 6.3\,\mathrm{m/s}$.

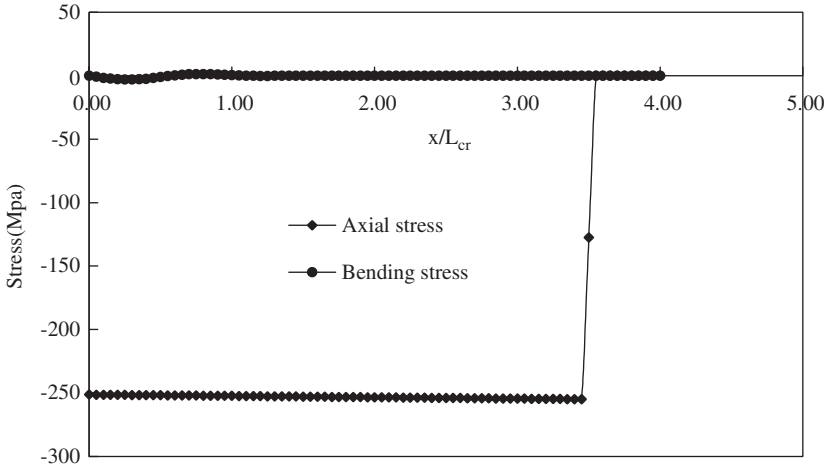

Fig. 14. Axial stress and bending stress in Ni–Cr steel bar, $\mu = 0.005$, $\tau = 3.5$.

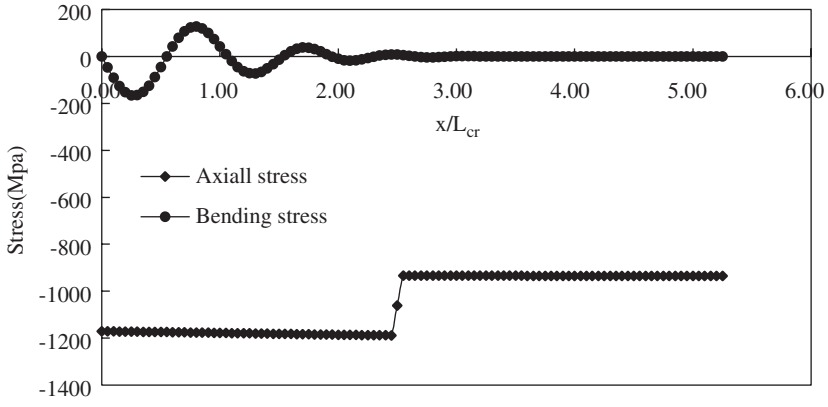

Fig. 15. Axial stress and bending stress in Ni–Cr steel bar, $\mu = 0.005$, $\tau = 23.5$.

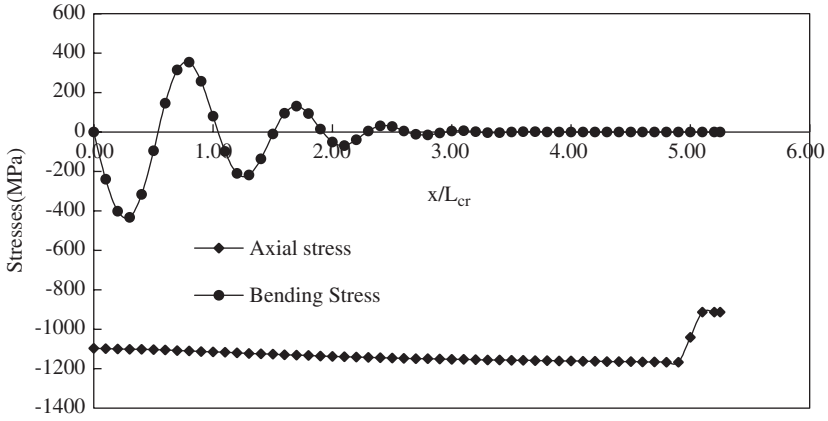

Fig. 16. Axial stress and bending stress in Ni–Cr steel bar, $\mu = 0.005$, $\tau = 26$.

bar material is high enough so that the axial stress in the bar would not exceed the yield stress, stress-time history at the impacted end is shown in Fig. 18. At the same time, Fig. 18 gives the comparison between the stress-time histories calculated for two cases with buckling and without buckling in the bar. It can be seen that the buckling deformations shorten sharply the duration of the loading before the first-time separation of the striking mass from the impacted end of the bar, and decreases the values of the axial stress in the bar, in comparison with the case where there is no buckling deformation.

6. Conclusion

By use of the finite difference method, the non-linear equations governing the elastic dynamic post-buckling deformations are solved for the two types of axial impact buckling problems of

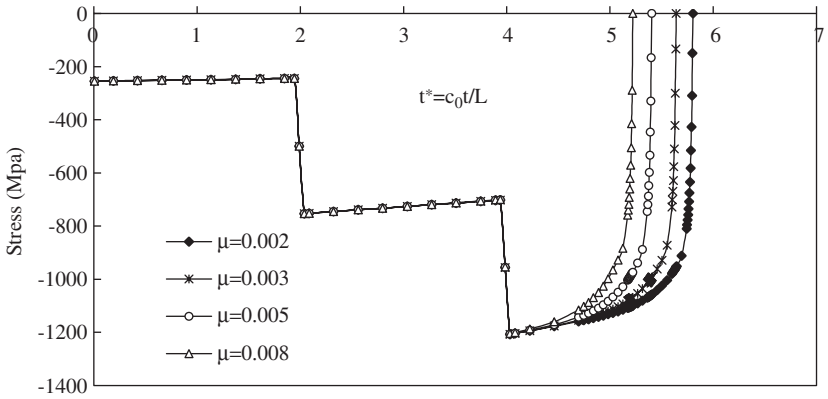

Fig. 17. Stress-time histories at the impacted end of Ni–Cr steel bar before the first-time separation of the striking mass from the impacted end.

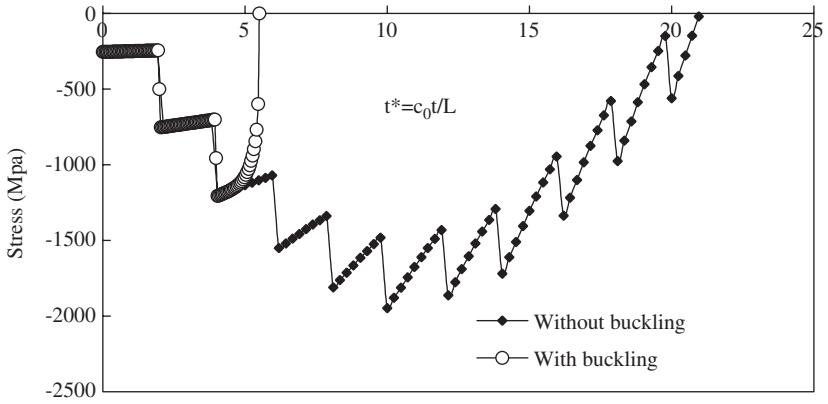

Fig. 18. Influence of buckling on the stress-time histories at the impacted end of Ni–Cr steel bar.

slender straight bars. The initial buckling mode with a small amplitude parameter, given by the twin-characteristic-parameter solution, is adopted as the initial condition of the non-linear post-buckling solution. Particular attention is paid to the mechanism of growth and spread of dynamic buckling deformation in the bar and the interaction between the axial stress wave and the buckling deformation in the process of impact.

For the slender straight bar subjected to axial impact with high velocity, the buckling deformation is initiated with the lowest mode of one half-wave near the impacted end, and the critical buckling length corresponding to the initial buckling mode is far shorter than the entire length of the bar. After buckling, the buckling deformation spreads forward and develops into a series of higher modes corresponding to different post-buckling stages, owing to the propagation of axial stress wave in the process of impact loading. The half-wave related to the initial buckling mode remains fixed in position, and the position corresponding to the half-wave front of the initial buckling mode, transforms into the wave-valley of the next half-wave of the higher

post-buckling mode, so that the length of the first half-wave near the impact end for the post-buckling deformation is shorter than that of the initial buckling mode.

The small amplitude parameter μ of the initial buckling deflection has little influence on the shape of the post-buckling deflection profile, but it needs a longer time t for the initial buckling mode with the smaller value of μ to develop into the post-buckling mode with the same amplitude.

The obvious unloading of the axial stress wave appears in the region close to the impacted end when the post-buckling deflection has already become large enough in this region. For the bar impacted by a traveling mass, the post-buckling deformations shorten sharply the duration of the loading before the first-time separation of the striking mass from the impacted end, and decreases significantly the values of the axial stress in the bar, in comparison with the case there is no buckling deformation in the bar.

Acknowledgements

This work is supported by Grant no. 10272114 of National Natural Science Foundation of China.

References

[1] Koning C, Taub J. Impact buckling of thin bars in the elastic range hinged at both ends. Luftfanrtforschung 1933;10(2):55–64 (translated as NACA TN 748 in 1934).
[2] Meier JH. On the dynamics of elastic buckling. J Aero Sci 1945;12:433–40.
[3] Gerard G, Becker H. Column behavior under conditions of impact. J Aero Sci 1952;19:58–65.
[4] Davidson JF. Buckling of struts under dynamic loading. J Mech Phys Solids 1953;2:54–66.
[5] Hoff NJ. The dynamics of the buckling of elastic columns. J Appl Mech 1953;17:68–74.
[6] Hutchinson JW, Budiansky B. Dynamic buckling estimates. AIAA 1966;4:525–30.
[7] Sevin E. On the elastic bending of columns due to dynamic axial forces including effects of axial inertia. J Appl Mech 1960;27:125–31.
[8] Lindberg HE. Impact buckling of a thin bar. ASME J Appl Mech 1965;32:315–22.
[9] Hayashi T, Sano Y. Dynamic buckling of elastic bars; 2nd report; the case of high velocity impact. Bull JSME 1972;15:1176–84.
[10] Lee LHN. Dynamic buckling of an inelastic column. Int J Solids Struct 1981;17:271–9.
[11] Ari-Gur J, Weller T, Singer J. Experimental and theoretical studies of columns under axial impact. Int J Solids Struct 1982;18:619–41.
[12] Housner JM, Knight Jr NF. The dynamic collapse of a column impacting a rigid surface. AIAA J 1983;21:1187–95.
[13] Lindberg HE, Florence AL. Dynamic pulse buckling-theory and experiment, Defence Nuclear Agency, Washington, Contract No. DNA 001-78-0287 (1983); Martinus Nijhoff, Norvell, MA, 1987.
[14] Simitses GJ. Instability of dynamically-loaded structures. Appl Mech Rev 1987;40:1403–8.
[15] Simitses GJ. Dynamic stability of suddenly loaded structures. New York: Springer; 1989.
[16] Jones N. Structural impact. Cambridge: Cambridge University Press; 1989.
[17] Karagiozova D, Jones N. Dynamic elastic–plastic buckling phenomena in a rod due to axial impact. Int J Impact Eng 1996;18:919–47.
[18] Hong Hao, Hee Kiat Cheong, Shijie Cui. Analysis of imperfect column buckling under intermediate velocity impact. Int J Solids Struct 2000;37:5297–313.

[19] Ülo Lepic. Dynamic buckling of elastic–plastic beams including effects of axial stress waves. Int J Impact Eng 2001;25:537–52.
[20] Wang, Anwen, Tian, Wenying. Twin-characteristic-parameter solution for dynamic buckling of columns under elastic compression wave. Int J Solids Struct 2002;39:861–77.
[21] Wang, Anwen, Tian, Wenying. Characteristic-value analysis for plastic dynamic buckling of columns under elastoplastic compression waves. Int J Non-Linear Mech 2003;38:615–28.
[22] Wang, Anwen, Tian, Wenying. Twin-characteristic-parameter solution of axisymmetric dynamic plastic buckling for cylindrical shells under compression waves. Int J Solids Struct 2003;40:3157–75.
[23] Wang, Anwen, Tian, Wenying. Twin-characteristic-parameters analysis for elastic dynamic buckling of thin cylindrical shells under axial step loading. Int J Impact Eng 2005;31:643–66.